*R*esearch in
*A*stronomy and
*A*strophysics

The electromagnetic and gravitational-wave radiations of X-ray transient CDF-S XT2

Hou-Jun Lü[1]⋆, Yong Yuan[1], Lin Lan[1], Bin-Bin Zhang[2,3], Jin-Hang Zou[4] and En-Wei Liang[1]

[1] Guangxi Key Laboratory for Relativistic Astrophysics, School of Physical Science and Technology, Guangxi University, Nanning 530004, China; *lhj@gxu.edu.cn*
[2] School of Astronomy and Space Science, Nanjing University, Nanjing 210093, China
[3] Key Laboratory of Modern Astronomy and Astrophysics (Nanjing University), Ministry of Education, Nanjing 210093, China
[4] Space Science and Technology, Hebei Normal University, Shijiazhuang 050000, China

Abstract Binary neutron star (NS) mergers may result in remnants of supra-massive or even stable NS, which have been supported indirectly by observed X-ray plateau of some gamma-ray burst (GRB) afterglows. Recently, Xue et al. (2019) discovered an X-ray transient CDF-S XT2 that is powered by a magnetar from merger of double NS via X-ray plateau and following stepper phase. However, the decay slope after the plateau emission is slightly larger than the theoretical value of spin-down in electromagnetic (EM) dominated by losing its rotation energy. In this paper, we assume that the feature of X-ray emission is caused by a supra-massive magnetar central engine for surviving thousands of seconds to collapse into a black hole. Within this scenario, we present the comparisons of the X-ray plateau luminosity, break time, and the parameters of magnetar between CDF-S XT2 and other short GRBs with internal plateau samples. By adopting the collapse time to constrain the equation of state (EOS), we find that three EOSs (GM1, DD2, and DDME2) are consistent with the observational data. On the other hand, if the most released rotation energy of magnetar is dominated by GW radiation, we also constrain the upper limit of ellipticity of NS for given EOS, and its range is $[0.32 - 1.3] \times 10^{-3}$. Its GW signal cannot be detected by Advanced LIGO or even for more sensitive Einstein Telescope in the future.

Key words: stars: magnetars

1 INTRODUCTION

The merger of a binary neutron star (NS) system is thought to be potential sources of producing both gravitational wave (GW) and associated electromagnetic (EM) signals (Berger 2014 for review). One solid case of producing a GW signal and associated EM (GW170817 and GRB 170817A, as well as kilonova AT 2017gfo), is already detected by Advanced LIGO (aLIGO), VIRGO, and other telescopes (Abbott et al. 2017; Goldstein et al. 2017; Coulter et al. 2017; Zhang et al. 2018). However, the remnants of double NS merger remain an open question.

From the theoretical point of view, there are four different types of merger remnants that are dependent on the total mass of the system and the poorly known NS equation of state (EOS; Rosswog et al. 2000; Dai et al. 2006; Fan & Xu 2006; Metzger et al. 2010; Rezzolla et al. 2011; Giacomazzo & Perna 2013; Zhang 2013; Lasky et al.

2014; Li et al. 2016). (1) a promptly formed black hole (Hotokezaka et al. 2011); (2) a hyper-massive NS, which can be survived for ∼ 100 ms before collapsing into a black hole (Baumgarte et al. 2000; Shibata & Taniguchi 2006; Palenzuela et al. 2015); (3) a supra-massive NS, which is supported by rigid rotation and survives for seconds to hours (Dai et al. 2006; Rowlinson et al. 2010; Hotokezaka et al. 2013; Zhang 2014; Lü et al. 2015; Gao et al. 2016; Kiuchi et al. 2018); (4) a stable NS (Dai & Lu 1998; Zhang & Mészáros 2001; Yu et al. 2010; Metzger et al. 2011; Bucciantini et al. 2012; Lü & Zhang 2014).

Recently, Xue et al. (2019) discovered an X-ray transient CDF-S XT2 that is associated with a galaxy at redshift $z = 0.738$, and its X-ray light curve is consistent with magnetar central engine model which is originated from double neutron star merger. The magnetar parameters are inferred by invoking the its X-ray plateau and followed decay segment in their work, and found that they are

---

⋆ Corresponding author

consistent with the parameters of magnetar in typical short GRBs. However, the decay slope after the plateau emission is slightly larger than the theoretical value of magnetar spin-down. On the other hand, a lower efficiency ($\eta = 0.001$) is adopted to estimate the parameters of magnetar for this transient in Xue et al. (2019). Here, we assume that the feature of X-ray emission is caused by a supra-massive magnetar central engine for surviving thousands of seconds to collapse into a black hole. Within this scenario, most rotation energy of magnetar may be dissipated in two ways. One is that the most of rotation energy is transformed into kinetic energy with injecting pulsar wind (Xiao & Dai 2019). The other possibility is that most of the rotational energy was carried away via the strong gravitational wave radiation (Fan et al. 2013; Lasky & Glampedakis 2016; Lü et al. 2018). In this paper, by considering two scenarios of rotation energy loss of magnetar for post-merger (i.e., EM dominated or GW dominated), we infer the surface magnetic field and initial period of NS, and constrain the EOS and ellipticity of NS, as well as detection probability of GW.

This paper is organized as follows. The empirical fitting of X-ray light curve for transient CDF-S XT2 is presented in Section 2. Some comparisons between CDF-S XT2 and other short GRBs with an internal plateau, as well as EOS are shown in Section 3. In Section 4, we constrain the ellipticity of NS, and calculate the detection probability of GW. The conclusions, along with some discussions, are presented in Section 5. Throughout this paper, a concordance cosmology with parameters $H_0 = 71$ km s^{-1} Mpc^{-1}, $\Omega_M = 0.30$, and $\Omega_\Lambda = 0.70$ is adopted.

2 LIGHT CURVE FIT AND CENTRAL ENGINE OF CDF-S XT2

2.1 Light Curve Fit of CDF-S XT2

The X-ray data of CDF-S XT2 observed by Chandra within energy band 0.3–10 keV are taken from Xue et al. (2019). We perform a temporal fit to the light curve with a smooth broken power law model, which is expressed as

$$L = L_0 \left[\left(\frac{t}{t_b} \right)^{\omega \alpha_1} + \left(\frac{t}{t_b} \right)^{\omega \alpha_2} \right]^{-1/\omega}, \qquad (1)$$

where $t_b(2525 \pm 242)$ s is the break time, $L_b = L_0 \cdot 2^{-1/\omega} = (1.28 \pm 0.16) \times 10^{45}$ erg s^{-1} is the luminosity at the break time t_b, $\alpha_1 = (0.09 \pm 0.11)$ and $\alpha_2 = (2.43 \pm 0.19)$ are decay indices before and after the break, respectively. The ω describes the sharpness of the break. The larger the ω parameter, the sharper the break, and $\omega = 3$ is fixed for the light curve fitting. An IDL routine named "mpfitfun.pro" is employed for our fitting (Markwardt
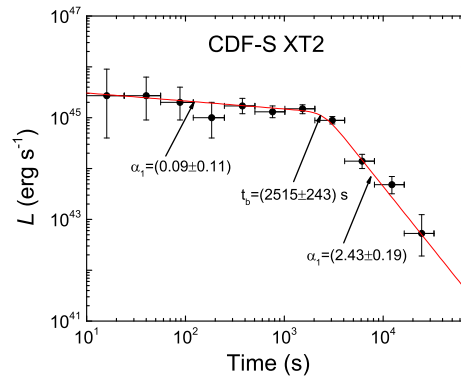
Fig. 1 X-ray light curve of CDF-S XT2. The *red solid line* is the fit with smooth broken power-law model.

2009). This routine performs a Levenberg-Marquardt least-squares fit to the data for a given model to optimize the model parameters. The light curve fit is shown in Figure 1.

2.2 Central Engine of CDF-S XT2

X-ray transient CDF-S XT2 associated with a galaxy at redshift $z = 0.738$ lies in the outskirts of its star-forming host galaxy with a moderate offset from the galaxy center, and there is no significant source-like gamma-ray emission signal above background. The observed properties are similar to those of other typical short GRBs, but in off-axis observed (Xue et al. 2019). On the other hand, the estimated event rate density of this event is similar to double NS merger rate density inferred from the detection of GW170817, suggesting that the progenitor of this event is likely from double NS merger (Xue et al. 2019). Moreover, the observed X-ray plateau of CDF-S XT2 is consistent with wind dissipation of magnetar central engine, and it indicates that the remnants of such double NS mergers should be either supra-massive NS or stable NS. However, the decay slope after the plateau emission ($t^{-2.43}$) is slightly larger than the theoretical value of spin-down (t^{-2}) in EM dominated by losing its rotation energy. Here, we assume that the feature of X-ray emission is caused by a supra-massive magnetar central engine for surviving thousands of seconds to collapse into a black hole.

In order to compare the properties of CDF-S XT2 with other short GRBs with an internal plateau, Figure 2 shows the correlation between break luminosity (L_b) and collapse time ($\tau_{\mathrm{col}} = t_b/(1 + z)$), as well as the distributions of L_b and τ_{col}. We find that the CDF-S XT2 falls into the 2σ deviation in $L_b - \tau_{\mathrm{col}}$ diagram, suggesting that the other short GRBs with internal plateau samples shared a similar central engine with the CDF-S XT2. However, the distributions of luminosity and collapse time of the
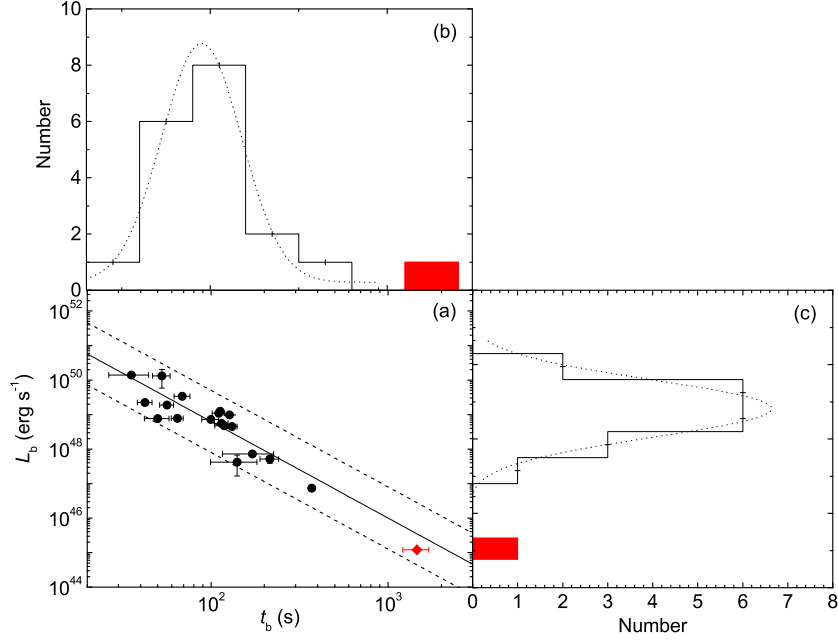
Fig. 2 (a): X-ray plateau luminosity (L_0) as a function of collapse time (t_{col}) for short GRBs with internal plateau (*black dots*) and X-ray transient CDF-S XT2 (*red diamond*). The *black solid line* is the the best fit with a power-law model, and the two *dashed lines* mark the 2σ region of the correlation, respectively. (b) and (c): distributions of t_{col} and L_0 with best-fit Gaussian profiles, respectively.

CDF-S XT2 is much lower and longer than other short GRBs with internal plateau samples, respectively. It may be caused by the directions of observations (i.e., on and off-axis with short GRBs and the CDF-S XT2), or having different populations of magnetars.

If we believe that a supramassive NS is a potential candidate central engine of CDF-S XT2, then one interesting question is: what is the energy loss channel of the rotating magnetar, dominated by magnetic dipole or GW radiation? We will discuss more details for the rotation energy loss of magnetar dominated by EM or GW radiations.

3 THE ROTATION ENERGY LOSS OF MAGNETAR VIA EM EMISSION

3.1 The Derived Parameters of Magnetar

The energy reservoir of a millisecond magnetar is the total rotation energy, which reads as

$$E_{rot} = \frac{1}{2}I\Omega^2 \simeq 2 \times 10^{52} \text{ erg } M_{1.4}R_6^2 P_{-3}^{-2} ,\qquad (2)$$

where I is the moment of inertia, Ω, P, R, and M are the angular frequency, rotating period, radius, and mass of the neutron star, respectively. The convention $Q = 10^x Q_x$ in cgs units is adopted. A magnetar spinning down loses its rotational energy via both magnetic dipole torques (L_{EM}) and GW (L_{GW}) radiations (Zhang & Mészáros 2001; Fan et al. 2013;
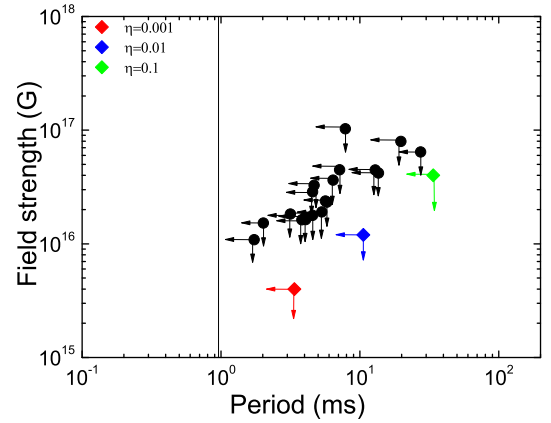
Fig. 3 Inferred magnetar parameters, initial spin period P_0 vs. surface polar cap magnetic field strength B_p derived for short GRBs with internal plateau (*black dots*) and X-ray transient CDF-S XT2 (*diamond*) with $\eta = 0.1, 0.01$ and 0.001. The *vertical solid line* is the break-up spin period limit for a neutron star (Lattimer & Prakash 2004).

Giacomazzo & Perna 2013; Lasky & Glampedakis 2016; Lü et al. 2018),

$$-\frac{dE_{rot}}{dt} = -I\Omega\dot{\Omega} = L_{total} = L_{EM} + L_{GW}$$
$$= \frac{B_p^2 R^6 \Omega^4}{6c^3} + \frac{32GI^2\epsilon^2\Omega^6}{5c^5}, \qquad (3)$$

where B_p is the surface magnetic field at the pole and $\epsilon = 2(I_{xx} - I_{yy})/(I_{xx} + I_{yy})$ is the ellipticity describing how large of the neutron star deformation. $\dot{\Omega}$ is the time
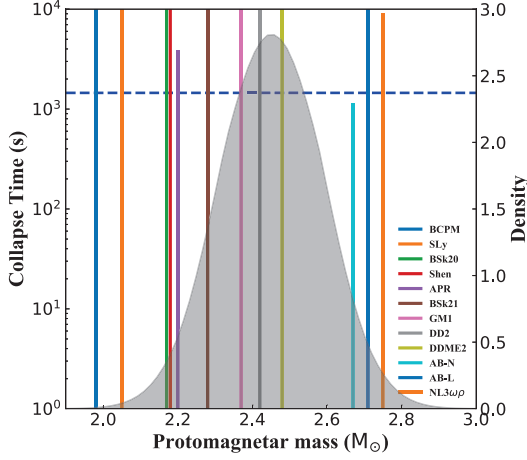
Fig. 4 Collapse time as a function of the protomagnetar mass of CDF-S XT2 for different EOS (*color lines*). The *shaded region* is the protomagnetar mass distribution derived from the total mass distribution of the Galactic NSCNS binary systems. The *horizontal dashed line* is the collapse time in the rest frame.
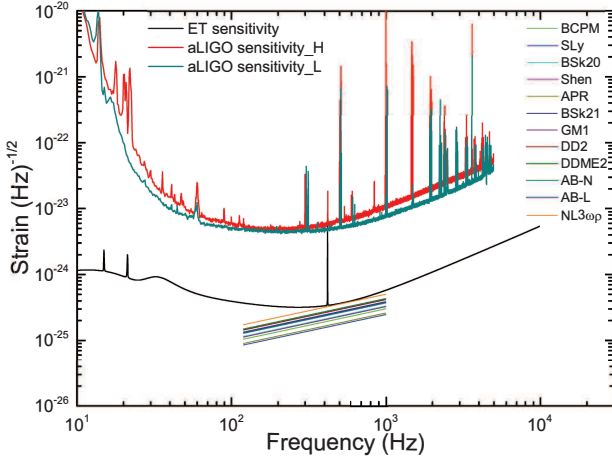
Fig. 5 Gravitational-wave strain evolution with frequency for CDF-S XT2 with different EOS at distances $D_L = 4480$ Mpc (*color lines*). The *black solid line* is the sensitivity limits for ET, and the *red* and *dark cyan solid lines* are are the sensitivity limits for aLIGO-Hanford and aLIGO-Livingston, respectively. The data of noise curve are taken from the website: *https://git.ligo.org/lscsoft/bilby/-/tree/master/bilby/gw/detector_curves*.

derivative of the angular frequency. One can find that for a magnetar with given R and I, its L_{EM} depends on B_p and Ω, and L_{GW} depends on ϵ and Ω.

If the rotation energy loss of magnetar is dominated by EM emission, one has

$$L_{EM} \simeq -I\Omega\dot{\Omega} = \frac{\eta B_p^2 R^6 \Omega^4}{6c^3}, \qquad (4)$$

where η is the efficiency of converting the magnetar wind energy into X-ray radiation. The characteristic spin-down luminosity ($L_{EM,sd}$) and time scale ($\tau_{EM,sd}$) of magnetar can be given as

$$\begin{aligned} L_{EM,sd} &= \frac{\eta B_p^2 R^6 \Omega_0^4}{6c^3} \\ &\simeq 1.0 \times 10^{46} \text{ erg s}^{-1} (\eta_{-3} B_{p,15}^2 P_{0,-3}^{-4} R_6^6), \end{aligned} \qquad (5)$$

$$\begin{aligned} \tau_{EM,sd} &= \frac{3c^3 I}{B_p^2 R^6 \Omega_0^2} \\ &\simeq 2.05 \times 10^3 \text{ s } (I_{45} B_{p,15}^{-2} P_{0,-3}^2 R_6^{-6}), \end{aligned} \qquad (6)$$

where Ω_0 and P_0 are initial angular frequency and period at $t = 0$, respectively.

Within the magnetar central engine scenario, the observed plateau luminosity is closed to L_b, which is roughly equal to $L_{EM,sd}$, and $\tau_{EM,sd} > \tau_{col}$. One can derive the magnetar parameters B_p and P_0,

$$B_{p,15} = 2.05(\eta_{-3}^{1/2} I_{45} R_6^{-3} L_{EM,sd,46}^{-1/2} \tau_{EM,sd,3}^{-1}) \text{ G}, \quad (7)$$

$$P_{0,-3} = 1.42(\eta_{-3}^{1/2} I_{45}^{1/2} L_{EM,sd,46}^{-1/2} \tau_{EM,sd,3}^{-1/2}) \text{ s}. \quad (8)$$

As radiation efficiency η depends strongly on the injected luminosity and wind saturation Lorentz factor (Xiao & Dai 2019). By adopting the lower limit of $\tau_{EM,sd}$, we derive the upper limits of P_0 and B_p with different η values. One has $P_0 < 3.4 \times 10^{-3}$ s and $B_p < 4 \times 10^{15}$ G for $\eta = 0.001$, $P_0 < 10.6 \times 10^{-3}$ s and $B_p < 1.2 \times 10^{16}$ G for $\eta = 0.01$, and $P_0 < 33.8 \times 10^{-3}$ s and $B_p < 4 \times 10^{16}$ G for $\eta = 0.1$. Figure 3 shows the $B_p - P_0$ diagram for X-ray transient CDF-S XT2 with different η values, and compares with other short GRBs with an internal plateau sample taken from Lü et al. (2015). It seems that small P_0 required by supra-massive magnetar is needed for lower radiation efficiency, and estimated B_p of CDF-S XT2 is lower than other typical short GRB samples for smaller P_0. It may be either off-axis observations or a different population of CDF-S XT2 by comparing with short GRBs.

3.2 Equation of State of NS

The inferred collapsing time can be used to constrain the neutron star EOS (Lasky et al. 2014; Ravi & Lasky 2014; Lü et al. 2015). The basic formalism is as follows.

The standard dipole spin-down formula gives (Shapiro & Teukolsky 1983)

$$\begin{aligned} P(t) &= P_0(1 + \frac{4\pi^2}{3c^3} \frac{B_p^2 R^6}{IP_0^2} t)^{1/2} \\ &= P_0(1 + \frac{t}{\tau_{EM,sd}})^{1/2}. \end{aligned} \qquad (9)$$

The maximum NS mass for a non-rotating NS (M_{TOV}) can be derived for given EOS of NS. The maximum

Table 1 The Basic Parameters of EOS of NS

	M_{TOV} ($M_\odot$)	R (km)	I (10^{45} g cm^2)	$\hat{\alpha}$ (10^{-10} $s^{-\hat{\beta}}$)	$\hat{\beta}$	ϵ (10^{-3})	$h_{\mathrm{c}}(f)$ (10^{-25})
BCPM	1.98	9.94	2.86	3.39	–2.65	1.5	3.02
SLy	2.05	9.99	1.91	1.60	–2.75	1.8	2.47
BSk20	2.17	10.17	3.50	3.39	–2.68	1.3	3.34
Shen	2.18	12.40	4.68	4.69	–2.74	1.2	3.87
APR	2.20	10.0	2.13	0.303	–2.95	1.7	2.61
BSk21	2.28	11.08	4.37	2.81	–2.75	1.2	3.74
GM1	2.37	12.05	3.33	1.58	–2.84	1.4	3.26
DD2	2.42	11.89	5.43	1.37	–2.88	1.1	4.16
DDME2	2.48	12.09	5.85	1.966	–2.84	1.0	4.32
AB-N	2.67	12.90	4.30	0.112	–3.22	1.2	3.71
AB-L	2.71	13.70	4.70	2.92	–2.82	1.2	3.87
NL3$\omega\rho$	2.75	12.99	7.89	1.706	–2.88	0.89	5.02

gravitational mass (M_{max}) depends on spin period, read as (Lyford et al. 2003)

$$M_{\mathrm{max}} = M_{\mathrm{TOV}}(1 + \hat{\alpha}P^{\hat{\beta}}),\qquad(10)$$

where $\hat{\alpha}$, $\hat{\beta}$, and M_{TOV} depend on the EOS of NS.

As the neutron star spins down, the centrifugal force can no longer sustain the star, and the NS will collapse into a black hole. By using Equations (9) and (10), one can derive the collapse time as function of M_{p},

$$t_{\mathrm{col}} = \frac{3c^3 I}{4\pi^2 B_{\mathrm{p}}^2 R^6}[(\frac{M_{\mathrm{p}} - M_{\mathrm{TOV}}}{\hat{\alpha}M_{\mathrm{TOV}}})^{2/\hat{\beta}} - P_0^2]$$
$$= \frac{\tau_{\mathrm{EM,sd}}}{P_0^2}[(\frac{M_{\mathrm{p}} - M_{\mathrm{TOV}}}{\hat{\alpha}M_{\mathrm{TOV}}})^{2/\hat{\beta}} - P_0^2].\qquad(11)$$

Here, we consider 12 EOSs that are reported in the literature (Lasky et al. 2014; Ravi & Lasky 2014; Li et al. 2016; Ai et al. 2018). The basic parameters of those EOSs are shown in Table 1.

As noted, one can infer B_p, P_0, and t_{col} from the observations by adopting $\eta = 0.001$. Following the method of Lasky et al. (2014), a tight mass distribution of the our Galactic binary NS population is adopted (e.g., Valentim et al. 2011; Kiziltan et al. 2013), and one can infer the expected distribution of proto-magnetar masses, which is found to be $M_p = 2.46^{0.13}_{-0.15}\ M_\odot$. For X-ray transient CDF-S XT2, the lower limit of $\tau_{\mathrm{EM,sd}} = t_{\mathrm{col}}$ is derived. Figure 4 presents the collapse time (t_{col}) as a function of protomagnetar mass (M_p) for CDF-S XT2 with different EOS. Our results show that the GM1, DD2, and DDME2 models give an M_{p} band falling within the 2σ region of the protomagnetar mass distribution, so that the correct EOS should be close to those three models. The maximum mass for non-rotating NS in those three models are $M_{\mathrm{TOV}} = 2.37\ M_\odot$, 2.42 $M_\odot$, and 2.48 $M_\odot$, respectively.

4 THE ROTATION ENERGY LOSS OF MAGNETAR VIA GW RADIATION

A survived supra-massive NS central engine requires a faster spinning ($P_0 \sim 1$ ms) to support the gravitational

force (Fan et al. 2013; Gao et al. 2013; Yu et al. 2013; Zhang 2013; Ho 2016; Lasky & Glampedakis 2016). As mentioned above, the estimated periods of magnetar are considerably longer ($\eta = 0.01$ and 0.1) than that expected in the double neutron star merger model. It seems that η should be as low as 0.001 or even smaller to obtain the lower period of magnetar. If this is the case, the rotation energy loss of magnetar is either transformed to kinetic energy of outflow or dominated by GW radiation (Lan et al. 2020). Xiao & Dai (2019) present more details for the first situation. In this section, we focus on considering the most rotation energy of magnetar dissipated via GW radiation.

4.1 Constraining the Ellipticity of NS

Within GW dominated scenario, one has (Lü et al. 2018)

$$L_{\mathrm{GW}} \simeq -I\Omega\dot{\Omega} = \frac{32GI^2\epsilon^2\Omega^6}{5c^5}.\qquad(12)$$

The characteristic spin-down luminosity ($L_{\mathrm{GW,sd}}$) and time scale ($\tau_{\mathrm{GW,sd}}$) of NS can be given as

$$L_{\mathrm{GW,sd}} = \frac{32GI^2\epsilon^2\Omega_0^6}{5c^5}$$
$$\simeq 1.08\times 10^{48}\ \mathrm{erg\ s}^{-1}(I_{45}^2\epsilon_{-3}^2 P_{0,-3}^{-6}),\qquad(13)$$

$$\tau_{\mathrm{GW,sd}} = \frac{5c^5}{128GI\epsilon^2\Omega_0^4}$$
$$\simeq 9.1\times 10^3\ \mathrm{s}\ (I_{45}^{-1}\epsilon_{-3}^{-2}P_{0,-3}^4).\qquad(14)$$

The supra-massive NS of CDF-S XT2 has collapsed into the black hole before it is spin-down, so that one has $\tau_{\mathrm{GW,sd}} > \tau_{\mathrm{col}}$. Combining with Equation (14), the upper limit of ellipticity (ϵ) can be expressed as

$$\epsilon < 2.5\times 10^{-3} I_{45}^{-1/2} P_{0,-3}^2.\qquad(15)$$

The maximum value of ϵ for different EOS with $P_0 = 1$ ms are shown in Table 1. We find that those values are in the range of $[0.32-1.3]\times 10^{-3}$. This upper limit value is larger than the maximum elastic quadrupole deformation of

conventional neutron stars, but is comparable to the upper limit derived for crystalline color-superconducting quark matter (Lin 2007; Johnson-McDaniel & Owen 2013).

4.2 Detection Probability of a GW

If most of the rotation energy is released via GW radiation with a frequency f, the GW strain for a rotating neutron star at distance $D_{\rm L}$ can be expressed as

$$h(t) = \frac{4GI\epsilon}{D_{\rm L}c^4}\Omega(t)^2 . \tag{16}$$

The signal-to-noise ratio of optimal matched filter can be expressed as

$$\rho^2 = \int_{f_1}^{f_2} \frac{\tilde{f}^2(f)}{S_h(f)}df , \tag{17}$$

where f_1 and f_2 are the initial and final GW frequencies, respectively. $\tilde{h}(f)$ is the Fourier transform of $h(t)$, namely $\tilde{h}(f) = h(t)\sqrt{dt/df}$. $S_h(f)$ is the noise power spectral density of the detector (Lasky & Glampedakis 2016). The characteristic amplitude of GW from a rotating NS can be estimated as (Corsi & Mészáros 2009; Hild et al. 2011; Lasky & Glampedakis 2016; Lü et al. 2017)

$$
\begin{aligned}
h_{\rm c} &= fh(t)\sqrt{\frac{dt}{df}} = \frac{f}{D_{\rm L}}\sqrt{\frac{5GI}{2c^3f}} \\
&\approx 8.22 \times 10^{-24}\left(\frac{I}{10^{45}\,{\rm g\,cm^2}}\frac{f}{1\,{\rm kHz}}\right)^{1/2} \\
&\quad \times \left(\frac{D_{\rm L}}{100\,{\rm Mpc}}\right)^{-1} .
\end{aligned}
\tag{18}
$$

For X-ray transient CDF-S XT2, its redshift $z = 0.738$ corresponds to $D_{\rm L} \sim 4480$ Mpc. By adopting the frequency range of GW from $f = 120$ Hz to 1000 Hz, one can estimate the maximum value of the strain $h_{\rm c}$ for different EOS of NS. The estimated values of $h_{\rm c}$ are reported in Table 1. The maximum value of the strain $h_{\rm c}$ for NL3$\omega\rho$ is about 5×10^{-25}, which is about one order of magnitude smaller than the aLIGO sensitivity, and also less than more sensitive Einstein Telescope (ET; see Fig. 5). It means that even if the merger remnant of double NS of this transient is a millisecond massive NS, the post merger GW signal is undetectable when the rotation energy of the NS is taken away by the GW radiation.

5 CONCLUSIONS AND DISCUSSION

The X-ray transient CDF-S XT2 associated with a galaxy at redshift $z = 0.738$ lies in the outskirts of its star-forming host galaxy with a moderate offset from the galaxy center, and no significant source-like gamma-ray emission signal above background (Xue et al. 2019).

Moreover, the estimated event rate density of this event is similar to double NS merger rate density inferred from the detection of GW170817, and the observed X-ray plateau is consistent with wind dissipation of magnetar central engine. This observed evidence supports that the progenitor of this event is likely from double NS merger, and the remnants of such double NS merger should be either supra-massive NS or stable NS. Moreover, Xiao et al. (2019) proposed that both the light curve and spectral evolution of CDF-S XT2 can be well explained by the internal gradual magnetic dissipation process in an ultra-relativistic wind. Sun et al. (2019) also presented that this transient is only observed from different zone, defined as free zone where the X-ray emission from magnetar spin-down can escape freely. Alternatively, Peng et al. (2019) argued that this transient is possible from tidal disruption event.

The decay slope after the plateau emission of CDF-S XT2 ($t^{-2.43}$) is slightly larger than the theoretical value of spin-down (t^{-2}) in EM dominated by losing its rotation energy. In this work, we assume that the feature of X-ray emission is caused by a supra-massive magnetar central engine for surviving thousands of seconds to collapse into a black hole. Within this scenario, in order to compare the observed properties of X-ray emission between CDF-S XT2 and other short GRBs with an internal plateau, we show the correlation between break luminosity and collapse time, as well as the distributions of them. We find that the CDF-S XT2 falls into the 2σ deviation in $L_b - \tau_{\rm col}$ diagram, suggesting that the other short GRBs with internal plateau samples shared a similar central engine with the CDF-S XT2. However, the distributions of luminosity and collapse time of the CDF-S XT2 is much lower and longer than other short GRBs with internal plateau samples, respectively. It may be caused by the directions of observations (i.e., on- and off-axis with short GRBs and the CDF-S XT2), or having different populations of magnetars.

On the other hand, one considers two channels of rotation energy loss of supra-massive magnetar, one is EM dominated, and the other is GW dominated. Within the first scenario, we estimate the parameters of magnetar (i.e., $B_{\rm p}$ and P_0) for given different radiation efficiency, as well as constraining the EOS of NS. It seems that small P_0, which is required by supra-massive magnetar, needs a lower radiation efficiency, and estimated $B_{\rm p}$ of CDF-S XT2 is lower than other typical short GRBs samples for smaller P_0. Moreover, we find that three EOSs (GM1, DD2, and DDME2) are consistent with the observational data of CDF-S XT2. Within the second scenario, we constrain the upper limit of ellipticity of NS for given different EOS; it is range of $[0.32 - 1.3] \times 10^{-3}$. By calculating the possible GW radiation for different EOS, we find that its

GW radiation cannot be detected by aLIGO or even for more sensitive Einstein Telescope in the future.

References

Abbott, B. P., Abbott, R., Abbott, T. D., et al. 2017, ApJL, 848, L13

Ai, S., Gao, H., Dai, Z.-G., et al. 2018, ApJ, 860, 57

Baumgarte, T. W., Shapiro, S. L., & Shibata, M. 2000, ApJL, 528, L29

Berger, E. 2014, ARA&A, 52, 43

Bucciantini, N., Metzger, B. D., Thompson, T. A., & Quataert, E. 2012, MNRAS, 419, 1537

Corsi, A., & Mészáros, P. 2009, ApJ, 702, 1171

Coulter, D. A., Foley, R. J., Kilpatrick, C. D., et al. 2017, Science, 358, 1556

Dai, Z. G., & Lu, T. 1998, A&A, 333, L87

Dai, Z. G., Wang, X. Y., Wu, X. F., & Zhang, B. 2006, Science, 311, 1127

Fan, Y.-Z., Wu, X.-F., & Wei, D.-M. 2013, Phys. Rev. D, 88, 067304

Fan, Y.-Z., & Xu, D. 2006, MNRAS, 372, L19

Gao, H., Ding, X., Wu, X.-F., et al. 2013, ApJ, 771, 86

Gao, H., Zhang, B., & Lü, H.-J. 2016, Phys. Rev. D, 93, 044065

Giacomazzo, B., & Perna, R. 2013, ApJL, 771, L26

Goldstein, A., Veres, P., Burns, E., et al. 2017, ApJL, 848, L14

Hild, S., Abernathy, M., Acernese, F., et al. 2011, Classical and Quantum Gravity, 28, 094013

Ho, W. C. G. 2016, MNRAS, 463, 489

Hotokezaka, K., Kyutoku, K., Okawa, H., et al. 2011, Phys. Rev. D, 83, 124008

Hotokezaka, K., Kyutoku, K., Tanaka, M., et al. 2013, ApJL, 778, L16

Johnson-McDaniel, N. K., & Owen, B. J. 2013, Phys. Rev. D, 88, 044004

Kiuchi, K., Kyutoku, K., Sekiguchi, Y., & Shibata, M. 2018, Phys. Rev. D, 97, 124039

Kiziltan, B., Kottas, A., De Yoreo, M., & Thorsett, S. E. 2013, ApJ, 778, 66

Lan, L., Lü, H.-J., Rice, J., & Liang, E.-W. 2020, ApJ, 890, 99

Lasky, P. D., & Glampedakis, K. 2016, MNRAS, 458, 1660

Lasky, P. D., Haskell, B., Ravi, V., et al. 2014, Phys. Rev. D, 89, 047302

Lattimer, J. M., & Prakash, M. 2004, Science, 304, 536

Li, A., Zhang, B., Zhang, N.-B., et al. 2016, Phys. Rev. D, 94, 083010

Lin, L.-M. 2007, Phys. Rev. D, 76, 081502

Lü, H.-J., & Zhang, B. 2014, ApJ, 785, 74

Lü, H.-J., Zhang, B., Lei, W.-H., Li, Y., & Lasky, P. D. 2015, ApJ, 805, 89

Lü, H.-J., Zhang, H.-M., Zhong, S.-Q., et al. 2017, ApJ, 835, 181

Lü, H.-J., Zou, L., Lan, L., & Liang, E.-W. 2018, MNRAS, 480, 4402

Lyford, N. D., Baumgarte, T. W., & Shapiro, S. L. 2003, ApJ, 583, 410

Markwardt, C. B. 2009, in Astronomical Society of the Pacific Conference Series, 411, Astronomical Data Analysis Software and Systems XVIII, eds. D. A. Bohlender, D. Durand, & P. Dowler, 251

Metzger, B. D., Giannios, D., Thompson, T. A., et al. 2011, MNRAS, 413, 2031

Metzger, B. D., Martínez-Pinedo, G., Darbha, S., et al. 2010, MNRAS, 406, 2650

Palenzuela, C., Liebling, S. L., Neilsen, D., et al. 2015, Phys. Rev. D, 92, 044045

Peng, Z.-K., Yang, Y.-S., Shen, R.-F., et al. 2019, ApJL, 884, L34

Ravi, V., & Lasky, P. D. 2014, MNRAS, 441, 2433

Rezzolla, L., Giacomazzo, B., Baiotti, L., et al. 2011, ApJL, 732, L6

Rosswog, S., Davies, M. B., Thielemann, F. K., & Piran, T. 2000, A&A, 360, 171

Rowlinson, A., O'Brien, P. T., Tanvir, N. R., et al. 2010, MNRAS, 409, 531

Shapiro, S. L., & Teukolsky, S. A. 1983, Black Holes, White Dwarfs, and Neutron Stars: the Physics of Compact Objects

Shibata, M., & Taniguchi, K. 2006, Phys. Rev. D, 73, 064027

Sun, H., Li, Y., Zhang, B.-B., et al. 2019, ApJ, 886, 129

Valentim, R., Rangel, E., & Horvath, J. E. 2011, MNRAS, 414, 1427

Xiao, D., Zhang, B.-B., & Dai, Z.-G. 2019, ApJL, 879, L7

Xiao, D., & Dai, Z.-G. 2019, ApJ, 878, 62

Xue, Y. Q., Zheng, X. C., Li, Y., et al. 2019, Nature, 568, 198

Yu, Y.-W., Cheng, K. S., & Cao, X.-F. 2010, ApJ, 715, 477

Yu, Y.-W., Zhang, B., & Gao, H. 2013, ApJL, 776, L40

Zhang, B. 2013, ApJL, 763, L22

Zhang, B. 2014, ApJL, 780, L21

Zhang, B. B., Zhang, B., Sun, H., et al. 2018, Nature Communications, 9, 447

Zhang, B., & Mészáros, P. 2001, ApJL, 552, L35